SCIENTIFIC REPORTS

OPEN

SUBJECT AREAS:
MOLECULAR BIOLOGY
ENDOCRINOLOGY

Received
29 October 2014

Accepted
5 January 2015

Published
28 January 2015

Correspondence and requests for materials should be addressed to S.Z. (shuzhang89@hotmail.com) or M.J.X. (manjiangxie@hotmail.com)

* These authors contributed equally to this work.

Simulated microgravity inhibits L-type calcium channel currents partially by the up-regulation of miR-103 in MC3T3-E1 osteoblasts

Zhongyang Sun[1]*, Xinsheng Cao[1]*, Zhuo Zhang[2]*, Zebing Hu[1], Lianchang Zhang[1], Han Wang[1], Hua Zhou[1], Dongtao Li[3], Shu Zhang[1] & Manjiang Xie[1]

[1]The Key Laboratory of Aerospace Medicine, Ministry of Education, The Fourth Military Medical University, 710032, Xi'an, Shaanxi, China, [2]Department of Neurology, Tangdu Hospital, The Fourth Military Medical University, 710032, Xi'an, Shaanxi, China, [3]Center of Cardiology, Navy General Hospital, 100048, Beijing, China.

L-type voltage-sensitive calcium channels (LTCCs), particularly Cav1.2 LTCCs, play fundamental roles in cellular responses to mechanical stimuli in osteoblasts. Numerous studies have shown that mechanical loading promotes bone formation, whereas the removal of this stimulus under microgravity conditions results in a reduction in bone mass. However, whether microgravity exerts an influence on LTCCs in osteoblasts and whether this influence is a possible mechanism underlying the observed bone loss remain unclear. In the present study, we demonstrated that simulated microgravity substantially inhibited LTCC currents and suppressed Cav1.2 at the protein level in MC3T3-E1 osteoblast-like cells. In addition, reduced Cav1.2 protein levels decreased LTCC currents in MC3T3-E1 cells. Moreover, simulated microgravity increased miR-103 expression. Cav1.2 expression and LTCC current densities both significantly increased in cells that were transfected with a miR-103 inhibitor under mechanical unloading conditions. These results suggest that simulated microgravity substantially inhibits LTCC currents in osteoblasts by suppressing Cav1.2 expression. Furthermore, the down-regulation of Cav1.2 expression and the inhibition of LTCCs caused by mechanical unloading in osteoblasts are partially due to miR-103 up-regulation. Our study provides a novel mechanism for microgravity-induced detrimental effects on osteoblasts, offering a new avenue to further investigate the bone loss induced by microgravity.

The maintenance of bone mass and the development of skeletal architecture are dependent on mechanical stimulation. Numerous studies have shown that mechanical loading promotes bone formation in the skeleton, whereas the removal of this stimulus during immobilization or in microgravity results in reduced bone mass. Microgravity, which is the condition of weightlessness that is experienced by astronauts during spaceflight, causes severe physiological alterations in the human body. One of the most prominent physiological alterations is bone loss, which leads to an increased fracture risk. Long-term exposure to a microgravity environment leads to enhanced bone resorption and reduced bone formation over the period of weightlessness[1,2]. An approximately 2% decrease in bone mineral density after only one month, which is equal to the loss experienced by a postmenopausal woman over one year, occurs in severe forms of microgravity-induced bone loss[3]. Experimental studies have shown that real or simulated microgravity can induce skeletal changes that are characterized by cancellous osteopenia in weight-bearing bones[4,5], decreased cortical and cancellous bone formation[5–7], altered mineralization patterns[8], disorganized collagen and non-collagenous proteins[9,10], and decreased bone matrix gene expression[11]. Decreased osteoblast function has been thought to play a pivotal role in the process of microgravity-induced bone loss. Both in vivo and in vitro studies have provided evidence of decreased matrix formation and maturation when osteoblasts are subjected to simulated microgravity[12,13]. The mechanism by which microgravity, which is a form of mechanical unloading, has detrimental effects on osteoblast functions remains unclear and merits further research.

Unfortunately, conducting well-controlled in vitro studies in sufficient numbers under real microgravity conditions is difficult and impractical because of the limited and expensive nature of spaceflight missions. Thus several ground-based systems, particularly clinostats, have been developed to simulate microgravity using

cultured cells to investigate pathophysiology during spaceflight. A clinostat simulates microgravity by continuously moving the gravity vector before the cell has sufficient time to sense the gravity vector, therefore, sensing no weight would have effects on cells similar to those of weightlessness. This method is called gravity-vector averaging[14].

Calcium is an important osteoblast regulator, and calcium channels are clearly associated with the regulation of osteoblast functions. Voltage-sensitive calcium channels (VSCCs), particularly LTCCs that selectively allow Ca^{2+} to cross the plasma membrane, are key regulators of intracellular Ca^{2+} homeostasis in osteoblasts[15]. LTCCs are composed of the pore-forming α_1 subunit and the auxiliary $\alpha_2\delta$ and β subunits; LTCCs in osteoblasts are devoid of the γ subunit[16]. The α_1 subunit determines the fundamental properties of individual VSCCs and has four homologous domains, I–IV, each with six transmembrane segments that are linked by cytoplasmic loops with intracellular NH_2 and COOH termini[17]. Among the 10 known α_1 subunits, the L-type Cav1.2 α_{1C} subunit is the most abundant and is the primary site for Ca^{2+} influx into growing osteoblasts[15,18].

LTCCs, particularly Cav1.2 LTCCs, play fundamental roles in cellular responses to external stimuli, including mechanical forces and hormonal signals, in osteoblastic lineage bone cells[17,19]. Several lines of evidence have found that bone density increases[20] and that bone resorption decreases when these calcium channels are activated in osteoblasts[21]. The application of cyclic strain to the substratum results in the increased incorporation of calcium in Ros 17/2.8 cell cultures, and this response is diminished in the presence of verapamil, which is a blocker of LTCCs[22]. The administration of the LTCC antagonists verapamil and nifedipine can substantially suppress mechanical loading-induced increases in bone formation in rats, suggesting that LTCCs mediate mechanically induced bone adaptation in vivo[23]. The levels of the extracellular matrix proteins osteopontin and osteocalcin increased in periosteal-derived osteoblasts by applying strain alone or strain in the presence of the LTCC agonist Bay K8644 within 24 h post-load. This mechanically induced increase in osteopontin and osteocalcin was inhibited by nifedipine[24]. In addition, physiological hormones such as parathyroid hormone and activated vitamin D_3 also modulate bone calcium homeostasis via LTCCs[25,26]. Thus, LTCCs play important roles in regulating osteoblast function.

Recent studies have shown that many factors participate in LTCC regulation. MicroRNA (miRNA), which is a small non-coding RNA molecule, has become the subject of many studies and functions in the silencing and post-transcriptional regulation of gene expression[27,28]. miRNAs function via base-pairing with complementary sequences within mRNA molecules[29]. Thus, these mRNA molecules are silenced by one or more of the following processes: the cleavage of the mRNA strand into two pieces, the destabilization of the mRNA through the shortening of its poly (A) tail, and decreased translation efficiency of the mRNA into proteins by ribosomes[29,30]. miR-1[31,32], miR-137[33,34], miR-328[35], miR-155[36], miR-145[37], and miR-103[38] participate in regulating Cav1.2 expression in several types of cells, whereas their functions in osteoblasts have not been confirmed.

Taken together, these data suggest that LTCCs have an important role in osteoblast function and that LTCCs are highly sensitive to mechanical stimulation[39]. In addition, LTCCs in osteoblasts may be regulated by miRNAs. However, to our knowledge, whether microgravity exerts an influence on LTCCs in osteoblasts and the possible mechanisms underlying this effect remain unclear. In the present study, we tested the hypothesis that simulated microgravity inhibits LTCCs in osteoblasts using patch-clamp analyses of whole-cell Ca^{2+} currents in MC3T3-E1 osteoblast-like cells under simulated microgravity and normal gravity conditions. In addition, we used quantitative real-time PCR (QPCR) and specific immunostaining approaches to examine the effects of simulated microgravity on Cav1.2 subunit expression. Moreover, we assessed the role of miR-103 in mediating the expression of the Cav1.2 subunit and the properties of LTCCs in osteoblasts.

Results

Simulated microgravity attenuates the Bay K8644-induced increase in the intracellular calcium concentration ($[Ca^{2+}]_i$). We performed calcium imaging to test for changes in $[Ca^{2+}]_i$ induced by Bay K8644 to determine whether simulated microgravity can affect LTCCs in MC3T3-E1 cells. The fluorescence intensity increased substantially within one second after the application of 10 μM Bay K8644 to the culture solution (Figure 1a and 1b). However, the effect of Bay K8644 on intracellular calcium dramatically decreased when the cells were pretreated with simulated microgravity (Figure 1c and 1d). The change in the fluorescence intensity ratio ($R = [(F_{max} - F_0)/F_0] \times 100\%$) of the control group was 2.48 ± 0.52, and the ratio of the simulated microgravity group was 1.57 ± 0.23. The difference between the ratios of the two groups is statistically significant ($P < 0.05$, Figure 1e). In addition, 75.3% ± 9.7% of the cells under simulated microgravity conditions and 80.7% ± 4.6% of the cells in the control group responded to Bay K8644 when the cells were screened for $[Ca^{2+}]_i$ changes, as shown in Figure 1f. The difference in the percentage of cells responding to Bay K8644 between the two groups was not statistically significant ($P > 0.05$).

Simulated microgravity reduces LTCC currents in osteoblasts. Electrophysiological recordings were performed on trypsinized cells to further confirm the influence of simulated microgravity on LTCCs in MC3T3-E1 cells. Figure 2 illustrates typical whole-cell LTCC currents recorded from osteoblasts from the control (Figure 2a) and simulated microgravity (Figure 2b) groups. The results show a reduction in LTCC currents due to simulated microgravity in the absence or presence of Bay K8644. The peak inward current was recorded at +10 mV for both control and simulated microgravity cells. The application of 10 μM Bay K8644 caused the current amplitude to increase by approximately 2-fold and to activate more steeply and at more negative potentials, whereas the application of 1 μM nifedipine suppressed the inward currents almost completely (Figure 2a and 2b). These properties suggest that the recorded inward currents were Ba^{2+} currents through LTCCs.

Because cell size may affect the current amplitude, the currents were normalized for membrane capacitance (C_m) as an indirect measurement of cell size and were expressed in picoampere (pA) per picofarad (pF). The inward currents were smaller at all command potentials in simulated microgravity compared with the control group regardless of whether the LTCCs were activated by Bay K8644 (Figure 2c and 2d. The I–V relation, which was expressed in terms of current density, was calculated using the estimated C_m). The LTCC current densities of the MC3T3-E1 cells of the simulated microgravity group were considerably smaller compared with those of the control group (Figure 2e). The mean peak current densities at +10 mV in the simulated microgravity and control groups were −2.41 ± 0.38 and −3.52 ± 0.48 pA/pF, respectively ($P < 0.05$, Figure 2e). The application of 10 μM Bay K8644 caused the maximum inward current density to increase by 1.5-fold, with no change in the maximal activation voltage (Figure 2f). The mean peak current densities in cells of the simulated microgravity and control groups were −3.24 ± 0.32 and −5.43 ± 0.49 pA/pF, respectively ($P < 0.05$, Figure 2f), in the presence of Bay K8644, indicating an approximately 2-fold decrease in sensitivity to Bay K8644 in the simulated microgravity group compared with the control.

Simulated microgravity down-regulates Cav1.2 but up-regulates its transcript level. The alteration of LTCC current and activity involves several significant components. The L-type Cav1.2 subunit is known to play a central role in the regulation of both LTCC current and activity; however, the roles of Cav1.2 in

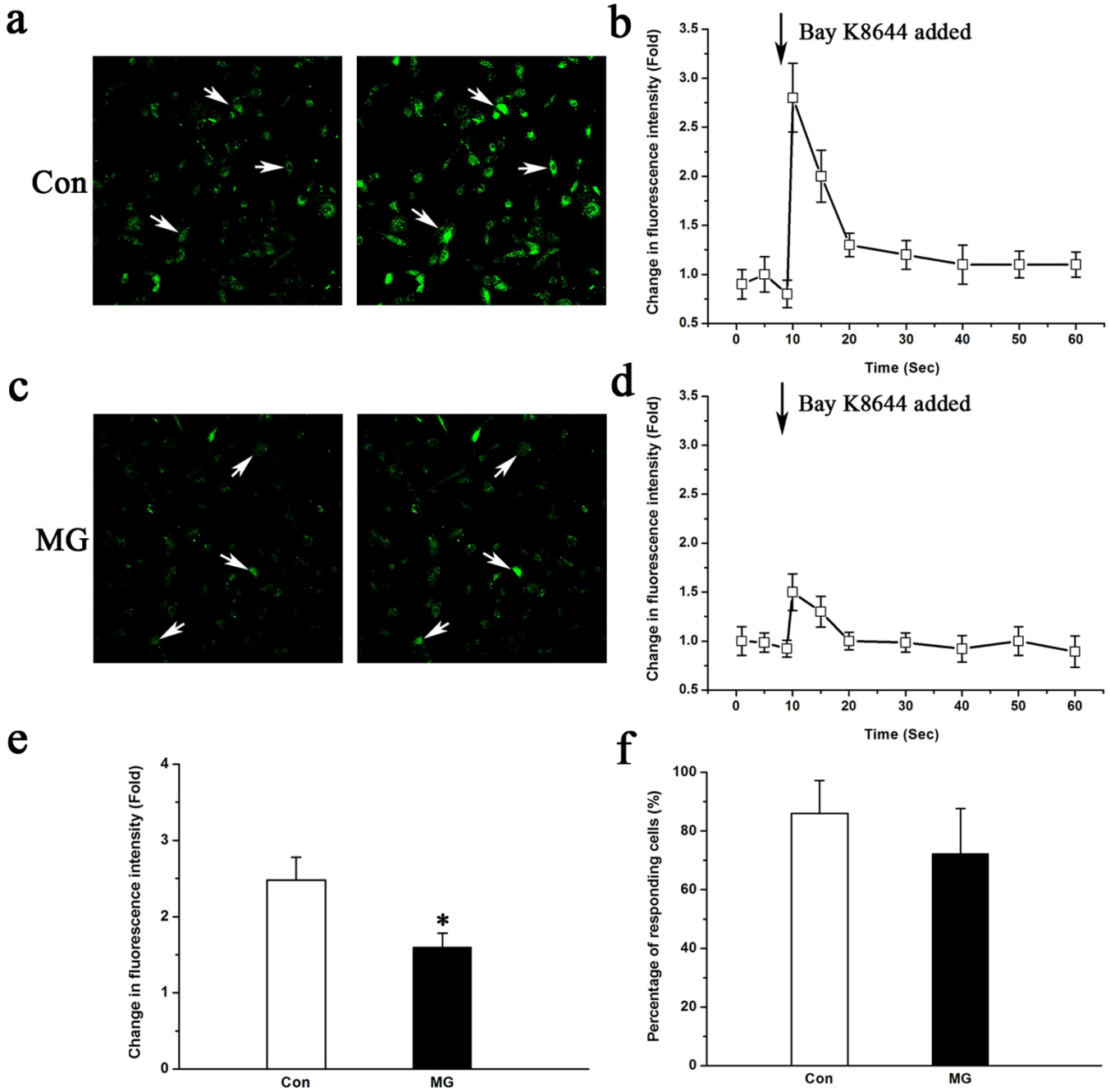

Figure 1 | Effects of simulated microgravity (MG) on changes in $[Ca^{2+}]_i$ induced by Bay K8644. (a) Effect of Bay K8644 on $[Ca^{2+}]_i$ in control (Con) cells: *left*, a representative picture of $[Ca^{2+}]_i$; *right*, a representative picture of $[Ca^{2+}]_i$ for cells treated with Bay K8644; twenty cells were measured in each experiment. (b) A representative curve of $[Ca^{2+}]_i$ changes in MC3T3-E1 cells treated with Bay K8644. (c) Effect of Bay K8644 on $[Ca^{2+}]_i$ in cells of the simulated microgravity group: *left*, a representative picture of $[Ca^{2+}]_i$; *right*, a representative picture of $[Ca^{2+}]_i$ for cells treated with Bay K8644; twenty cells were measured in each experiment. (d) A representative curve of $[Ca^{2+}]_i$ changes induced by Bay K8644 in cells of the simulated microgravity group. (e) Difference in $[Ca^{2+}]_i$ with Bay K8644 treatment in control and simulated microgravity-pretreated cells ($n = 4$, $\alpha = 0.05$, $^*P = 0.022$). (f) Differences in the percentage of cells responding to Bay K8644 between the control and simulated microgravity groups ($n = 4$, $\alpha = 0.05$, $P = 0.076$). Each group shown is from four experiments with a cumulative analysis of 80 cells total. Bars represent the mean ± s.d. with two-tailed Student's *t*-test against control samples.

mediating the function of LTCCs under real or simulated microgravity conditions remain unclear. Therefore, we investigated whether Cav1.2 expression was altered under simulated microgravity conditions. We performed immunostaining for the Cav1.2 subunit in MC3T3-E1 cells to study the expression and cellular localization of Cav1.2 in cells under simulated microgravity conditions. In Figure 3, immunostaining for the Cav1.2 subunit in MC3T3-E1 cells is shown before and after exposure to 48 h of simulated microgravity conditions (Figure 3). Control cells stained for Cav1.2 showed abundant plasma membrane and intracellular localization, particularly on the cell surface (Figure 3b and 3c). In contrast, the 48 h simulated microgravity conditions decreased immunostaining for Cav1.2 (Figure 3f and 3g). Intracellular staining persisted but was less intense than that observed in control cells, and the staining for Cav1.2 in the cell periphery markedly decreased (Figure 3f and 3g). Images were compared with cells that had been incubated with Fluor 488-conjugated secondary antibody in the absence of primary antibody to determine the specificity of staining (Figure 3d). The

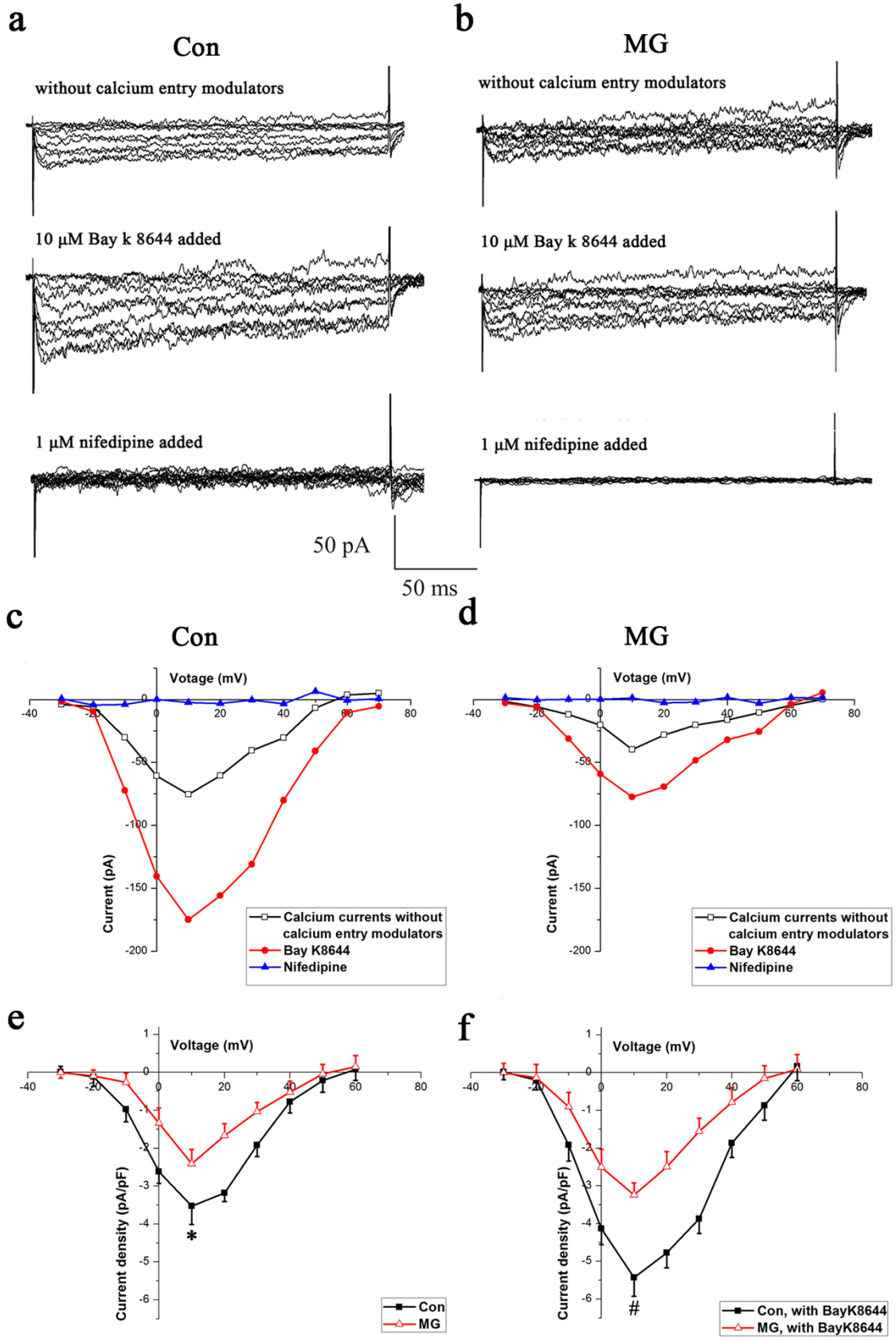

Figure 2 | LTCC currents in MC3T3-E1 from Con and MG groups. (a) and (b) Representative families of inward currents were recorded without Ca^{2+} entry modulators (*upper*) and in the presence of Bay K8644 (*middle*) or nifedipine (*lower*) from a holding potential of −40 mV for a Con cell and for a MG MC3T3-E1 cell. (c) and (d) I–V curves for a single cell under each condition. (e) and (f) Comparison of changes in LTCC current densities between Con (n = 16 cells) and MG cells (n = 13 cells), regardless of whether the LTCCs were activated by Bay K8644 ($\alpha = 0.05$, $^{*}P = 0.018$, $^{\#}P = 0.007$). The values are the mean ± s.d., and statistically significant differences were determined using a one-way ANOVA with a Bonferroni post hoc test.

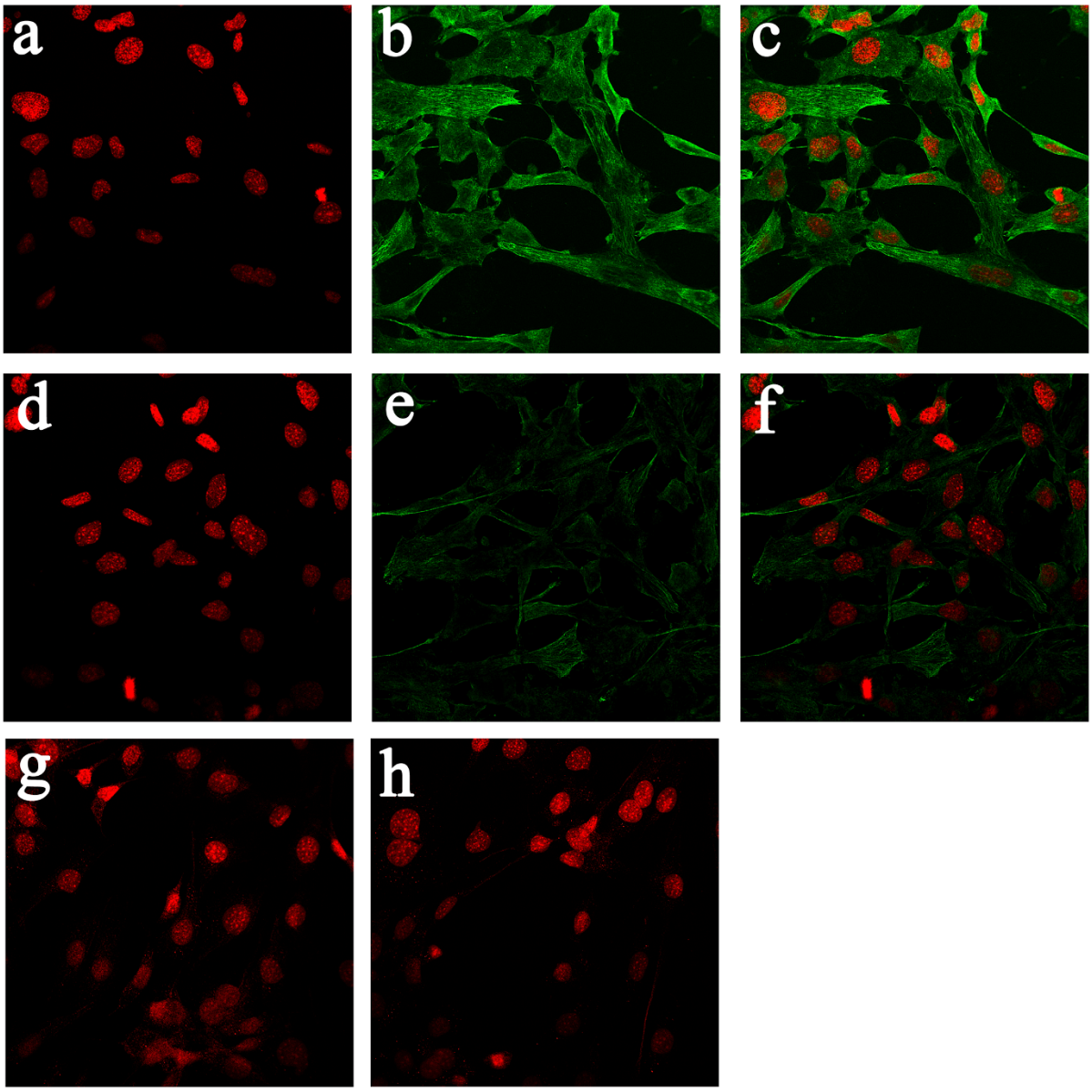

Figure 3 | Immunocytochemistry of Cav1.2 LTCC in MC3T3-E1 cells in response to 48 h under simulated microgravity conditions. (a), (b) and (c) Staining of MC3T3-E1 cells under normal gravity conditions with the nucleic acid dye ToPro3 (a), rabbit anti-Cav1.2 antibodies (b), (a) and (b) merged (c), with Alexa Fluor 488-conjugated anti-rabbit IgG as the secondary antibody. (d), (e) and (f) Simulated microgravity-treated MC3T3-E1 cells stained with the nucleic acid dye ToPro3 (d), rabbit anti-Cav1.2 antibodies (e), (d) and (e) merged (f), with Alexa Fluor 488-conjugated anti-rabbit IgG as the secondary antibody. (g) MC3T3-E1 cells incubated with competing peptides for anti-Cav1.2. Cultures incubated with the competing peptide displayed slight green staining and comparable levels of nuclear staining. (h) MC3T3-E1 cells incubated with Alexa Fluor 488-conjugated secondary antibody in the absence of primary antibody.

signal specificity for the antibody was determined by incubating MC3T3-E1 cells with competing peptide and anti-Cav1.2 antibody (Figure 3h). Western blot analyses were performed to further confirm the results of immunostaining for the Cav1.2 subunit in MC3T3-E1 cells regarding protein expression. Cav1.2 expression in the two groups is shown in Figure 4a. Cav1.2 expression significantly decreased by approximately 50% under simulated microgravity conditions compared with that of the horizontal rotation controls ($P < 0.05$, Figure 4a).

Cav1.2 mRNA expression was measured by QPCR in MC3T3-E1 cells treated for 48 h under simulated microgravity or control conditions. The QPCR results for the LTCCs expressed in MC3T3-E1 cells were normalized to untreated control values for each primer set to detect changes in expression levels. As shown in Figure 4b, Cav1.2 mRNA subunit transcription levels increased by 1.4-fold under 48 h of simulated microgravity conditions compared with that of control ($P < 0.05$). These data are in disagreement with the protein data, suggesting that certain mechanisms at the post-transcriptional level may play a role in regulating Cav1.2 expression.

Cav1.2 knockdown reduces calcium currents. We examined LTCC currents by knocking down Cav1.2 expression to further clarify whether the alterations in Cav1.2 expression are involved in the reduction of LTCC currents in osteoblasts. Western blotting was used to evaluate gene knockdown efficiency following siRNA transfection. As shown in Figure 5a, siRNA treatment resulted in an approximately 60% suppression of the protein at 48 h post-transfection, with significant suppression lasting up to 72 h ($P < 0.05$). Therefore, the cells were subjected to patch clamp at 48 h post-transfection, which is the period at which Cav1.2 expression

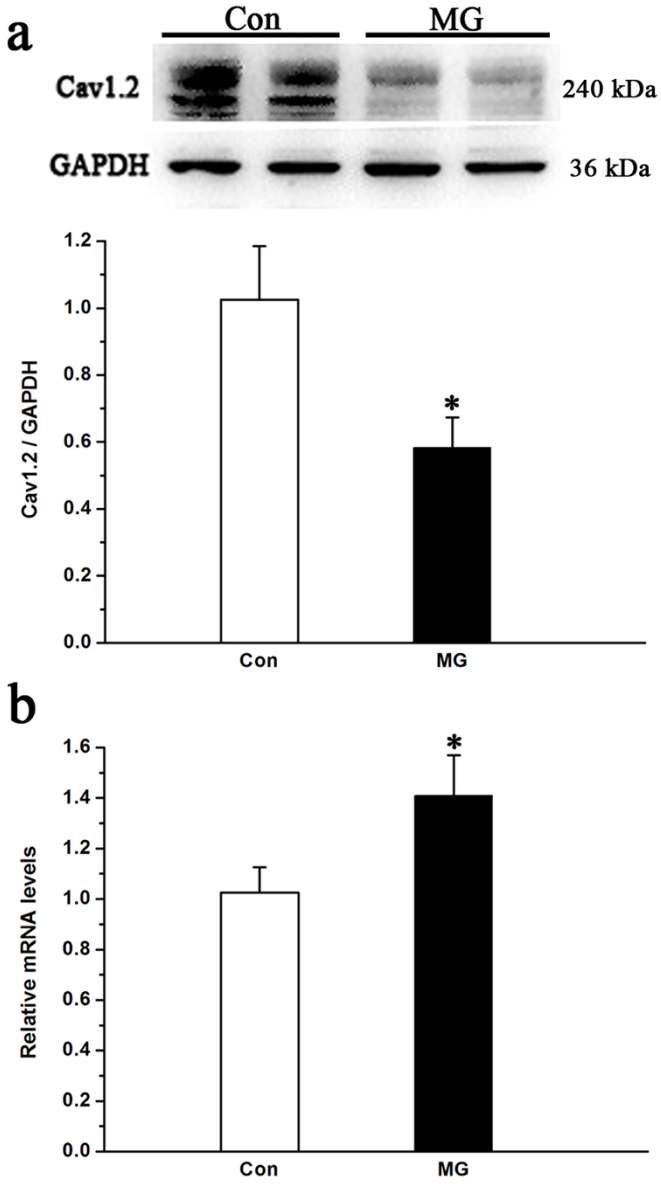

Figure 4 | Changes in the Cav1.2 subunit protein and mRNA expression levels in MC3T3-E1 cells under simulated microgravity conditions. (a) Western blot analysis of Cav1.2 expression from cell lysates from MC3T3-E1 under normal gravity and simulated microgravity conditions. The total protein loaded per lane was 40 μg; GAPDH detection on the same blots was used to verify equal loading among the various lanes (*upper*). Histogram showing the average data for the relative expression of Cav1.2 present in the cells from the Con and MG groups, which was quantified by the camera-based detection of emitted chemiluminescence (*lower*) (n = 4, $\alpha = 0.05$, $^*P = 0.019$). (b) QPCR analysis of changes in the relative Cav1.2 mRNA levels in MC3T3-E1 cells under simulated microgravity conditions (n = 6, $\alpha = 0.05$, $^*P = 0.032$). Bars represent the mean ± s.d. with two-tailed Student's *t*-test against control samples.

was maximally suppressed. LTCC current densities were significantly lower at all command potentials between cells receiving scrambled or Cav1.2 siRNA, regardless of whether the LTCCs were activated by Bay K8644 (Figure 5b and 5c). The difference in the mean peak current densities at +10 mV between the Cav1.2 knockdown (−1.58 ± 0.26 pA/pF) and the control cells (−2.76 ± 0.34 pA/pF) was significant ($P < 0.05$, Figure 5d). Moreover, in the presence of Bay K8644, the mean peak current densities in cells from knockdown and control cells were −2.72 ± 0.34 and −4.75 ± 0.44 pA/pF, respectively, and the difference between the two groups was significant ($P < 0.05$, Figure 5e).

miR-103 is up-regulated under simulated microgravity conditions. All six miRNAs that have been reported to mediate Cav1.2 expression were examined by QPCR to ascertain which miRNA family is relevant to the alteration in Cav1.2 expression under simulated microgravity conditions. Figure 6 shows that miR-103 was remarkably up-regulated in the simulated microgravity group compared with controls ($P < 0.05$). Other than miR-103, the remaining miRNAs showed no significant differences between the two groups ($P > 0.05$, Figure 6). These findings indicate that miR-103 may be involved in regulating Cav1.2 expression under simulated microgravity conditions.

miR-103 inhibition partially rescues the decrease in Cav1.2 induced by simulated microgravity. To confirm the effect of miR-103 on Cav1.2 expression under simulated microgravity conditions, a miR-103 inhibitor was transfected into MC3T3-E1 cells, and western blot analyses were performed to test for Cav1.2 expression. miR-103 expression was significantly down-regulated ($P < 0.05$, Figure 7a) in miR-103 inhibitor-transfected cells. Under simulated microgravity conditions, Cav1.2 expression significantly increased in miR-103 inhibitor-transfected cells compared with that of miR-103 negative control-transfected cells ($P < 0.05$, Figure 7b); however, Cav1.2 expression was not restored to control levels. In addition, the miR-103 inhibitor had no effects on Cav1.2 expression in cells under normal gravity conditions ($P < 0.05$, Figure 7b). These data suggest that miR-103 partially regulates Cav1.2 expression in MC3T3-E1 cells under simulated microgravity conditions.

A miR-103 inhibitor partially counteracts the decrease in LTCC currents induced by simulated microgravity. Next, the influence of miR-103 on LTCC currents was investigated to further assess the role of miR-103 on the expression of Cav1.2. Under normal gravity conditions, the inward currents did not differ between the negative control group (Figure 8a) and the miR-103 inhibitor group (Figure 8b). However, the inward currents were larger at all command potentials in the miR-103 inhibitor group (Figure 8d) compared with the negative control group (Figure 8c) under simulated microgravity conditions in the absence or presence of Bay K8644. The LTCC current densities in the miR-103 inhibitor-transfected cells were significantly larger compared with those of the negative control group under simulated microgravity conditions ($P < 0.05$, Figure 8e and 8f). The difference in the mean peak current densities at +10 mV between the miR-103 inhibitor group (−2.86 ± 0.33 pA/pF) and the negative control group (−2.02 ± 0.38 pA/pF) was significant ($P < 0.05$, Figure 8e). The application of 10 μM Bay K8644 caused the maximum inward current density to increase by 1.6-fold with no change in the maximal activation voltage. In the presence of Bay K8644, the mean peak current densities in osteoblasts from the two groups were −4.34 ± 0.43 and −2.93 ± 0.32 pA/pF, and the difference between two groups was significant ($P < 0.05$, Figure 8f). Similar to the finding for Cav1.2 expression, miR-103 inhibitor transfection could not restore the LTCC currents back to the control levels ($P < 0.05$, Figure 8e and 8f). Additionally, miR-103 inhibitor had no effects on the LTCC currents in cells under normal gravity conditions ($P > 0.05$, Figure 8e and 8f).

Discussion

Although the catabolic effects of microgravity on bone have been well documented, the mechanism by which mechanical unloading results in osteoblast dysfunction remains unclear. We have postulated that simulated microgravity has adverse effects on osteoblasts by inhibiting LTCCs. Our results indicate that simulated microgravity substantially inhibits LTCCs in MC3T3-E1 osteoblast-like cells by suppressing Cav1.2 expression. Furthermore, we demonstrated that the up-regulation of miR-103 that is induced by simulated micro-

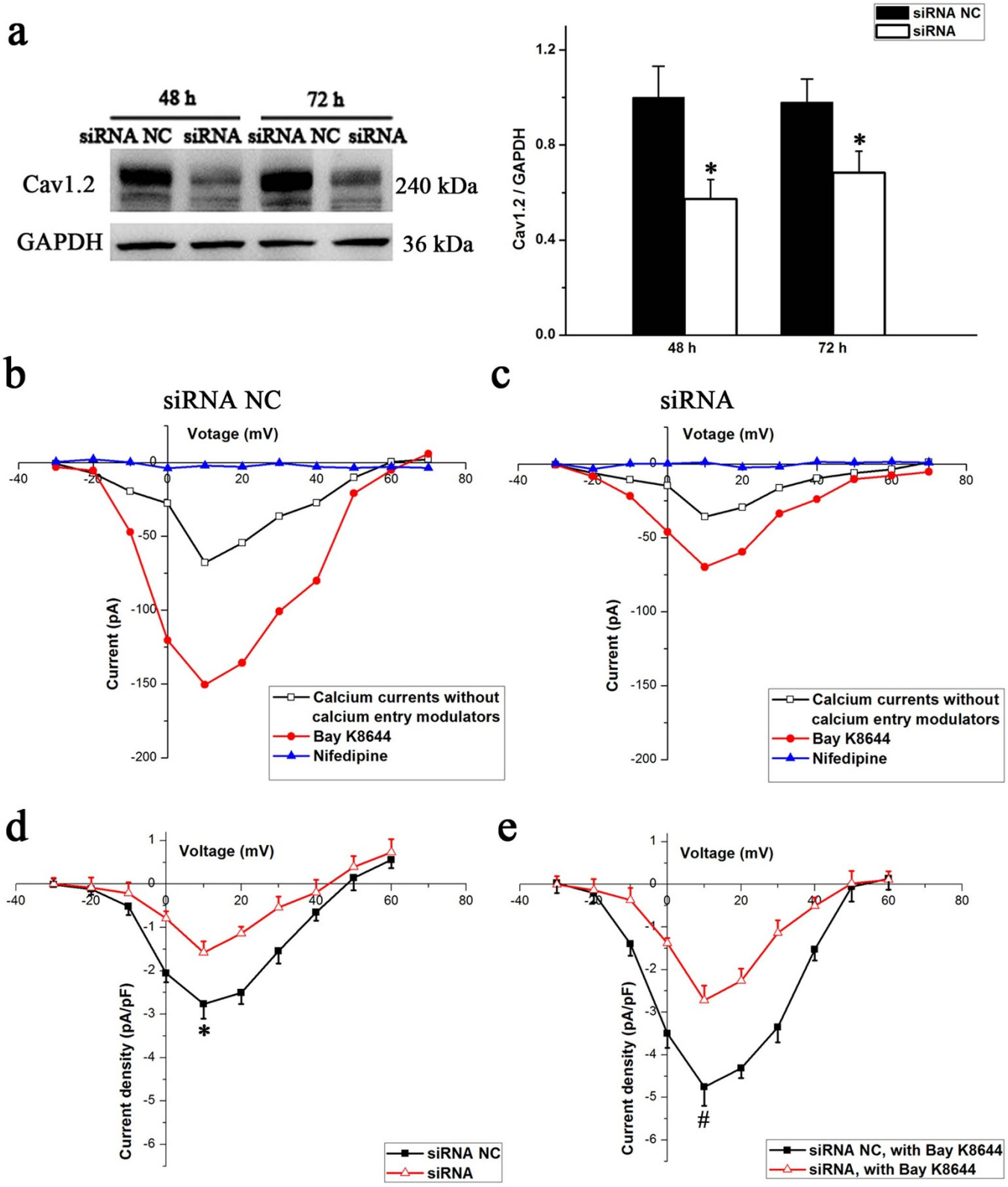

Figure 5 | Effects of changes in the Cav1.2 subunit protein on LTCC currents. (a) MC3T3-E1 cells were transfected with Cav1.2 siRNA and negative control (NC) siRNA (70 nM) for 12 h, followed by postincubation for 48 and 72 h additional hours. Western blot analysis indicates the magnitude and duration of Cav1.2 subunit suppression (n = 4, $\alpha = 0.05$, $^{*}P = 0.016$). Bars represent the mean ± s.d. with two-tailed Student's *t*-test against control samples. (b) I–V curves for the siRNA NC group. (c) I–V curves for the siRNA group. (d) and (e) Comparison of changes in the LTCC current densities in MC3T3-E1 cells of the siRNA NC group (n = 12 cells) and the siRNA group (n = 13 cells), regardless of whether the LTCCs were activated by Bay K8644 ($\alpha = 0.05$, $^{*}P = 0.036$, $^{\#}P = 0.013$). The values are the mean ± s.d., and statistically significant differences were determined using a one-way ANOVA with a Bonferroni post hoc test.

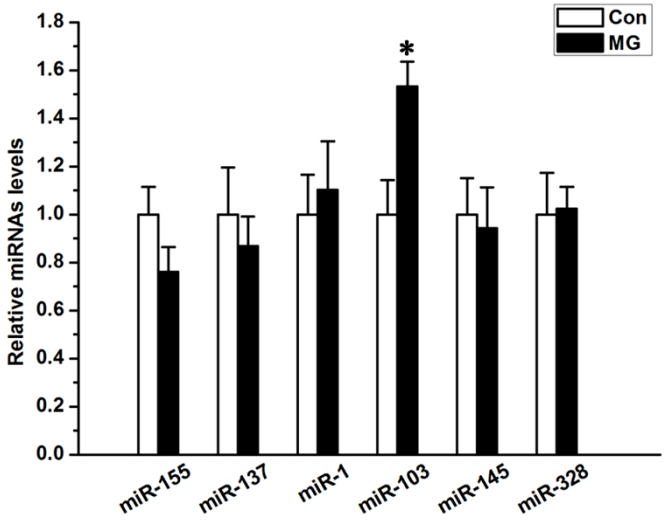

Figure 6 | Alteration of miRNAs in MC3T3-E1 cells under simulated microgravity conditions. QPCR analysis of changes in the expression of miR-155, miR-137, miR-1, miR-103, miR-145 and miR-328 in MC3T3-E1 cells simulated microgravity conditions (n = 6, $\alpha = 0.05$, $^{*}P = 0.021$). Bars represent the mean ± s.d. with two-tailed Student's *t*-test against control samples.

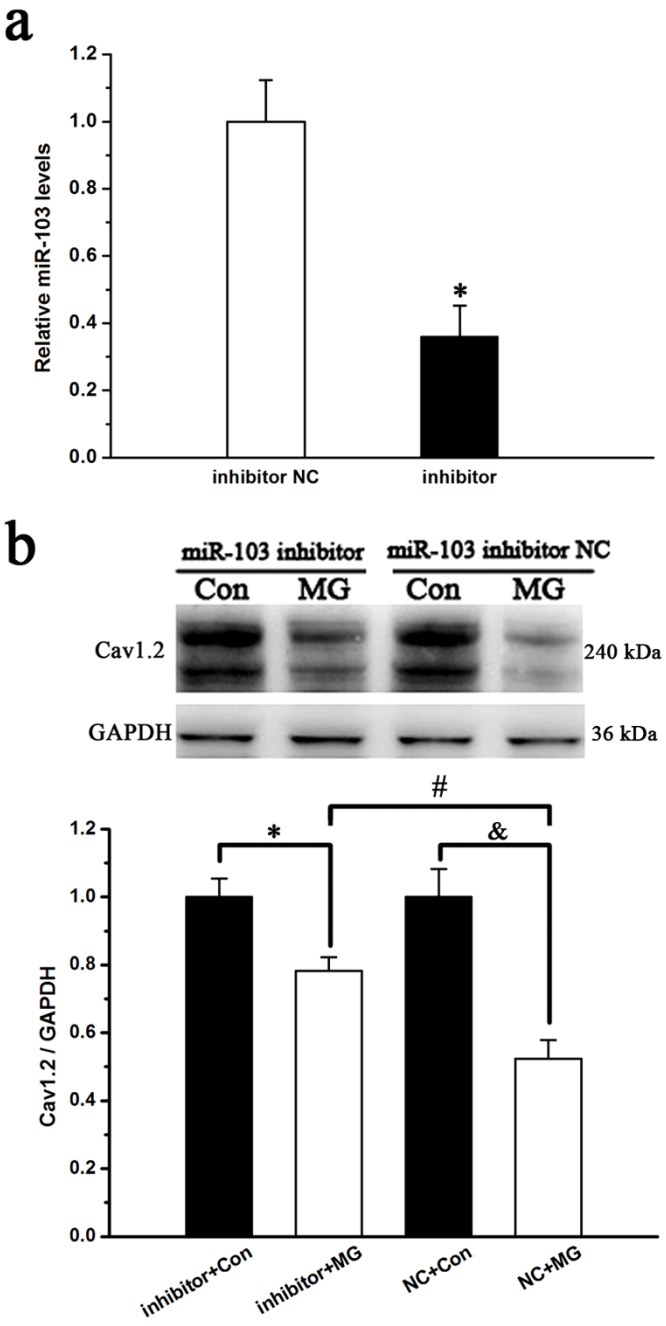

Figure 7 | Effects of miR-103 knockdown on Cav1.2 subunit expression under simulated microgravity conditions. (a) Knockdown of endogenous miR-103 by a miR-103 inhibitor in MC3T3-E1 cells (n = 4, $\alpha = 0.05$, $^{*}P = 0.016$). (b) Western blot analysis of the role of miR-103 in regulating the expression of the Cav1.2 subunit under simulated microgravity conditions (n = 4, $\alpha = 0.05$, $^{*}P = 0.022$, $^{\#}P = 0.017$, $^{\&}P = 0.016$). Bars represent the mean ± s.d. with two-tailed Student's *t*-test against control samples.

gravity is involved in the down-regulation of Cav1.2 expression and in the inhibition of LTCCs in MC3T3-E1 cells.

Orbital spaceflight has clearly demonstrated that the absence or the reduction of gravity has significant detrimental effects on astronauts. Health hazards in astronauts are represented by cardiovascular deconditioning and bone loss. Skeletal deconditioning, such as reduced bone mass, altered mineralization patterns and decreased bone matrix gene expression, has been described in astronauts and in rat models of simulated microgravity. The skeletal system impairment that is induced by mechanical unloading, which is one of the main limitations of long-term spaceflight, has received general attention by researchers[40]. LTCCs are involved in the production and release of paracrine/autocrine factors[41,42] and in changes in gene expression[43] in response to mechanical stimulation. Li et al. reported that LTCC inhibition significantly attenuates the bone formation that is associated with mechanical loading in rats and mice[44]. These findings suggest that LTCCs play important roles in the regulation of osteoblast function and bone metabolism. In the present study, we investigated the effects of simulated microgravity on LTCC currents in cultured MC3T3-E1 cells using whole-cell patch clamp recordings. By measuring inward currents, we found that simulated microgravity significantly reduced LTCC currents. This finding was also confirmed by calcium imaging, which showed that simulated microgravity significantly reduced Bay K8644-induced intracellular calcium increases. These observations are consistent with previous studies. Numerous bone anabolic regulatory factors, including parathyroid hormone[45,46], vitamin D_3[45], and mechanical stimuli[47,48], are able to activate and enhance LTCC currents. Therefore, microgravity, which is a form of mechanical unloading, may reduce LTCC currents in osteoblasts.

Many factors can regulate LTCCs. The major LTCC subunit in osteoblasts is Cav1.2[15,18]. Recent studies have shown that amyloid precursor protein (APP) inhibits LTCCs by down-regulating Cav1.2 expression in GABAergic inhibitory neurons[49]. Ronkainen et al. reported that LTCC currents in cardiomyocytes are suppressed by calcium-calmodulin-dependent protein kinase II (CaMKII) through the down-regulation of Cav1.2 expression[50]. Considering the inhibition of LTCC currents in MC3T3-E1 cells under simulated microgravity condition, we investigated Cav1.2 expression in these cells. Our findings showed that simulated microgravity markedly suppresses the expression of Cav1.2 in MC3T3-E1 cells. Then, we examined these currents following the knockdown of Cav1.2 expression to confirm that the reduction of Cav1.2 was involved in the alteration of LTCC currents in MC3T3-E1 cells. Our results demonstrated that the down-regulation of Cav1.2 expression notably reduces LTCC currents in MC3T3-E1 cells. These data suggested that the decreased activity of LTCCs in MC3T3-E1 cells under simulated microgravity condition could be attributed to a decreased amount of Cav1.2 channel proteins.

In addition to the APP and CaMKII studies mentioned above, other reports have investigating the regulation of the Cav1.2 channel

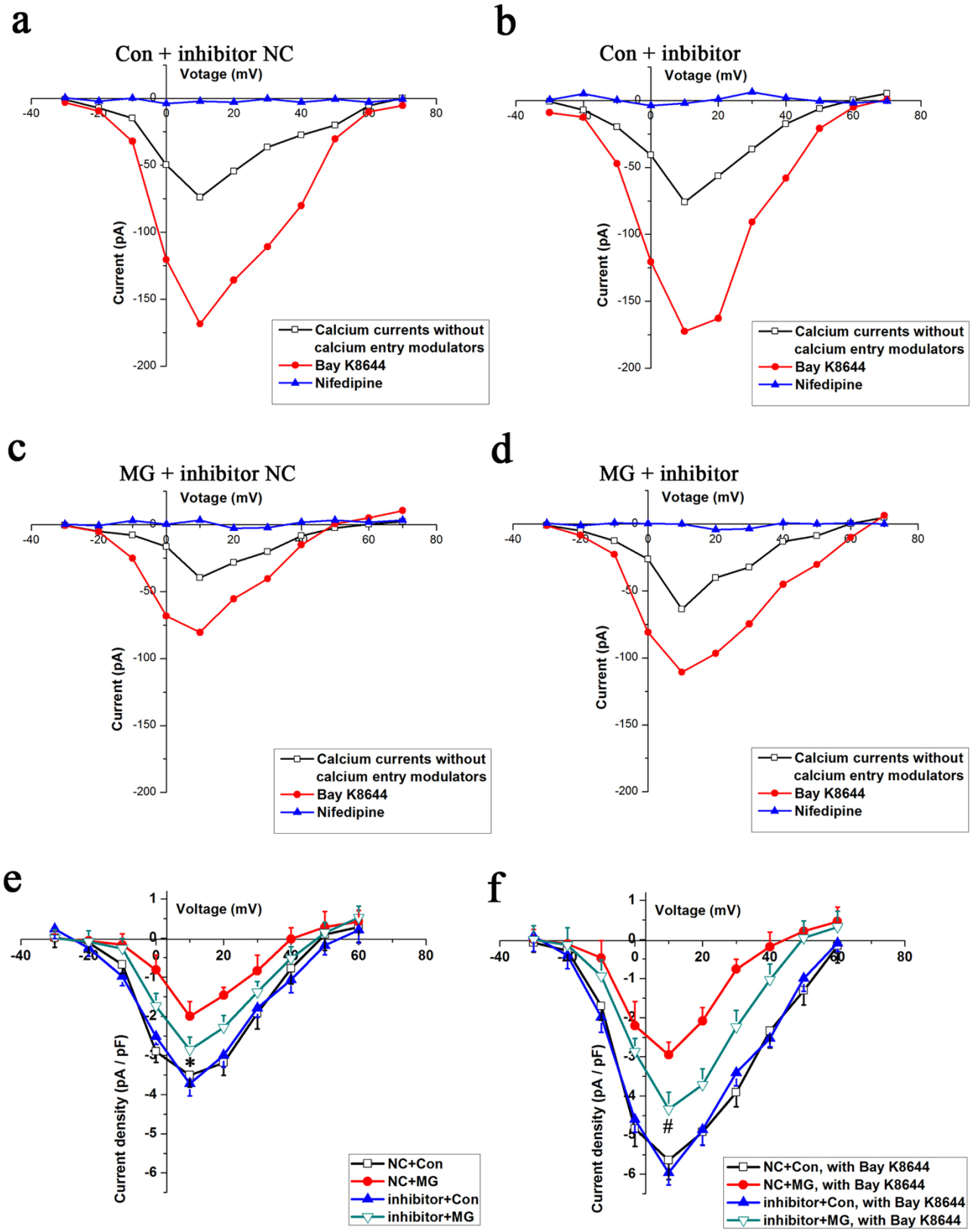

Figure 8 | Effects of miR-103 knockdown on LTCC currents in MC3T3-E1 cells under simulated microgravity conditions. (a) I–V curves for the Con + miR-103 inhibitor NC group. (b) I–V curves for the Con + miR-103 inhibitor group. (c) I–V curves for the MG + miR-103 inhibitor NC group. (d) I–V curves for the MG + miR-103 inhibitor group. (e) and (f) Comparison of changes in the LTCC current densities in cells of the miR-103 inhibitor NC + MG group (red, n = 12 cells) and the miR-103 inhibitor + MG group (green, n = 14 cells), regardless of whether the LTCCs were activated by Bay K8644 ($\alpha = 0.05$, $^{*}P = 0.032$, $^{\#}P = 0.006$). The values are the mean ± s.d., and statistically significant differences were determined using a one-way ANOVA with a Bonferroni post hoc test.

protein. For example, selenium deficiency increases oxidative stress levels in the mouse myocardium, which is positively related to the up-regulation of Cav1.2 genes and proteins[51]. Wang et al. demonstrated that Cav1.2 mRNA and protein levels increase in ROS cells following a 24-h incubation with a permeable analog of cAMP[52]. These experiments suggested that changes in Cav1.2 expression that are induced by different factors coincide with altered Cav1.2 mRNA expression. However, our findings indicated that increased Cav1.2 mRNA expression is not consistent with decreased Cav1.2 protein expression in MC3T3-E1 cells under simulated microgravity conditions. Therefore, this result suggested that a mechanism of post-transcriptional regulation might participate in regulating Cav1.2 protein expression.

miRNA, which is a small non-coding RNA molecule, has roles in RNA silencing and post-transcriptionally regulating gene expression. Recently, six miRNAs have been linked to the regulation of Cav1.2 expression under different experimental conditions using a luciferase-based reporter assay. *Cacna1c*, which encodes a LTCC Cav1.2 subunit, is the gene target of miR-137 during the regulation of adult neurogenesis and neuron maturation[33,34]. Other studies have shown that miR-1 is associated with heart defects and atrioventricular block through mediating Cav1.2 expression[31,32]. Lu et al. reported that miR-328 contributes to the adverse atrial electric remodeling in atrial fibrillation through targeting the L-type Ca^{2+} channel genes *Cacna1c* and *Cacnb1*, which encode for α_{1c} and β_1 subunits, respectively[35]. Moreover, miR-155[36], miR-145[37], and miR-103[38] have also been reported to play a crucial role in regulating Cav1.2 expression. We examined all six of these miRNAs by real-time PCR to determine which may be relevant to the altered Cav1.2 expression in MC3T3-E1 cells under simulated microgravity conditions. Our results showed that simulated microgravity increases miR-103 expression but has no effects on the other miRNAs. This finding indicated that miR-103 might be involved in regulating Cav1.2 expression under simulated microgravity conditions.

We studied the effects of treating MC3T3-E1 cells with a miR-103 inhibitor to further determine the role of miR-103 in regulating Cav1.2 expression under simulated microgravity conditions. Our data showed that miR-103 inhibition remarkably increased the expression of Cav1.2 subunits and LTCC currents in MC3T3-E1 cells under simulated microgravity conditions; however, this treatment could not completely counteract the decreases in Cav1.2 expression and LTCC currents that were induced by simulated microgravity. These results are consistent with the finding by Favereaux et al., who demonstrated that the knockdown or overexpression of miR-103 up- or down-regulates, respectively, the level of Cav1.2 expression in neurons[38]. miRNA functions in the post-transcriptional regulation of gene expression via base-pairing with mRNA molecules[29]. miRNA silences mRNA by one or more of the following processes: the cleavage of the mRNA strand into two pieces, the destabilization of the mRNA through the shortening of its poly (A) tail, and reduced translation efficiency of the mRNA into proteins by ribosomes[29,30]. In this study, simulated microgravity down-regulated Cav1.2 expression but up-regulated its transcript level, suggesting that miR-103 decreases Cav1.2 subunit expression by blocking the translation of the mRNA into protein. Collectively, these studies suggest that the up-regulation of miR-103 in simulated microgravity is at least partially involved in the regulation of Cav1.2 subunit expression and LTCC currents in MC3T3-E1 cells. In addition to the miRNAs mentioned, there have been other reports investigating Cav1.2 expression at post-transcriptional level. Recent studies have shown that Cav1.2 contain an endoplasmic reticulum retention motif in the proximal C-terminal region, and the Cavβ subunit has a role in regulating proteasomal degradation of this subunit[53]. Moreover, Rougier et al. showed that Nedd4-1 promotes the sorting of newly synthesized Cav1.2 for degradation by both the proteasome and the lysosome[54]. However, whether ubiquitination pathway or other possible mechanisms for regulating Cav1.2 expression at post-transcriptional level in osteoblasts under microgravity condition remain to be investigated.

In conclusion, simulated microgravity inhibits LTCCs in MC3T3-E1 cells via the suppression of Cav1.2 expression. Moreover, the down-regulation of Cav1.2 expression and the inhibition of LTCCs are partially related to the up-regulation of miR-103 induced by simulated microgravity. To our knowledge, this study is the first to demonstrate the relation between the inhibition of LTCCs and the up-regulation of miR-103 under conditions of simulated microgravity in MC3T3-E1 cells in vitro. This work may provide a novel mechanism of microgravity-induced adverse effects on osteoblasts, offering a new avenue to further investigate microgravity-induced bone loss. A more detailed analysis of the mechanisms accounting for the suppressive effect of simulated microgravity on Cav1.2 expression is under investigation.

Methods

Materials. Unless otherwise stated, all chemicals and reagents used in this study were obtained from Sigma Chemical Company.

Cell culture. Mouse osteoblast-like MC3T3-E1 cells were grown in α-minimum essential medium (α-MEM; Hyclone) containing 10% fetal calf serum (Hyclone), 100 U/ml penicillin G, and 100 mg/ml streptomycin. The cells were maintained in a humidified incubator at 37°C with 5% CO_2 and were subcultured every 72 h.

Clinorotation to simulate microgravity. The clinostat is an effective, ground-based tool that is used to simulate microgravity. The clinostat consists of two groups of turntables: one vertical turntable and one horizontal turntable. The vertical chambers rotate around the horizontal axis, which designates clinorotation. Clinorotation mimics certain aspects of a microgravity environment by nullifying the integrated gravitational vector through continuous averaging. The horizontal chambers rotate around the vertical axis, which designates rotational control. The cells were exposed to clinorotation for 48 h at 24 rpm. In the present study, the cells were seeded at a density of 1×10^5 cells on 2.5 cm × 3.0 cm coverslips that were placed in 6-well plates. After the cells grew for 24 h and adhered to the coverslips, the coverslips were inserted into the fixture of the chambers, which were subsequently filled with α-MEM with 10% FBS and aspirated to eliminate air bubbles. The chambers were divided into two groups: horizontal rotation control and clinorotation. The clinostat was placed in an incubator at 37°C[55,56].

Calcium imaging. After 48 h of incubation, the cells were loaded with Fluo-3-AM. For this manipulation, each chamber was washed twice with 1 ml of HEPES-buffered salt solution (HBSS). Following the wash, 5 μM Fluo-3-AM in HBSS was added, and the cells were incubated for 40 minutes in a 5% CO_2 humidified incubator in the dark. Then, changes in intracellular Ca^{2+} levels in individual cells were measured using a digital imaging system equipped with a laser confocal scanning microscope (FluoView 1000, Olympus). The cells were excited at a wavelength of 488 nm, and the emission fluorescence was recorded at 525 nm. Images were acquired at a rate of 1 s per frame for up to 1 min. Once the cells were focused and a stable baseline cytosolic calcium level was recorded, the HBSS was exchanged for a high potassium HBSS, which had 55 mM KCl instead of 6 mM and 70 mM NaCl instead of 120 mM. This high potassium HBSS also contained 10 μM Bay K8644[57].

Image analysis was performed using customized sequences from Bio-Rad Comos software and the confocal image analysis system. Changes in fluorescence were normalized by calculating the percent change ratio (R) from the resting level before stimulation using the equation $R = [(F_{max} - F_0)/F_0] \times 100\%$, where F_0 is the mean of several determinations of fluorescence intensity taken before the application of high potassium HBSS, and F_{max} is the maximum fluorescence intensity after 10 μM Bay K8644 was added[24].

Measurement of the LTCC currents. Whole-cell currents were recorded with an amplifier (CEZ-2300, Nihon Kohden) and a version interface (Axon Instruments) using patch clamp techniques. Command-voltage protocols and data acquisition were performed with pCLAMP software (version 8.0, Axon Instruments). Patch pipettes (tip resistance 2-6 MΩ when filled with a pipette solution) were fabricated on an electrode puller (Narishige) using borosilicate glass capillary tubing. Cell membrane capacitance (C_m) and access resistance (R_a) were estimated from the capacitive current transient evoked by applying a 20 mV pulse for 40 ms from a holding potential of −60 mV to −40 mV.

The cell was held at −40 mV and then stepped in 10 mV increments from −30 to 60 mV. Voltage steps were 250 ms in duration, and 2 s intervals were allowed between steps. Nonspecific membrane leakage and residual capacitive currents were subtracted using the p/4 protocol. Ba^{2+} replaced Ca^{2+} as the charge carrier to increase unitary currents, and the divalent cation concentration was elevated in the bath solution. Barium was used as a current carrier for two reasons: barium current through L-type channels is known to be larger than calcium currents; and barium inhibits potassium channel activation[58,59]. Two types of external solutions, solutions A

and B, were used. Solution A was used while making a gigaohm seal between the recording pipette and cell surface. This solution contained (in mM) 120 NaCl, 30 mannitol, 3 K_2HPO_4, 1 $MgSO_4$, 30 HEPES and was supplemented with 0.1% bovine serum albumin and 0.5% glucose, with the pH corrected to 7.4 with NaOH. After a seal of 2 GΩ was obtained, the perfusion fluid was changed to solution B during current recording. Solution B contained (in mM) 108 $BaCl_2$ and 10 HEPES, with the pH corrected to 7.6 with $Ba(OH)_2$. Cs^+ was used in the pipette solution to minimize outward K^+ current. The pipette solution contained (in mM) 150 CsCl, 5 EGTA, 10 HEPES, 5 Na_2ATP, and 10 D-glucose, with the pH adjusted to 7.2 with CsOH[24,58–60].

Immunocytochemistry and fluorescence microscopy. The detection of the Cav1.2 subunit was performed using a rabbit polyclonal antibody against Cav1.2, which was obtained from Alomone Laboratories. The cells were fixed in 4% (vol/vol) paraformaldehyde and then incubated in blocking buffer containing 5% (vol/vol) normal donkey serum, 0.3% (vol/vol) Triton X-100, and PBS to permeabilize and block nonspecific binding. The primary antibody was diluted 1 : 100 with 1% (vol/vol) normal donkey serum and 0.1% (wt/vol) BSA in PBS. Then, the cells were incubated in the dark for 1 h at room temperature using Alexa Fluor 488-conjugated (Invitrogen) secondary antibody (1 : 200). The cells were counterstained for 10 min in the dark with the nuclear dye ToPro3 (Molecular Probes), which was diluted 1 : 4,000 in PBS. The fluorescence intensity was analyzed using an inverted microscope linked to a confocal scanning unit (FluoView 1000, Olympus)[15].

Western blot analysis. The cells were lysed in RIPA buffer (Thermo) containing a protease inhibitor cocktail (Roche). Equal amounts of protein from each sample were added to a NuPage Bis-Tris polyacrylamide gel (Invitrogen) and run for 2 hours using MES SDS running buffer (Invitrogen). Then, the proteins were transferred to nitrocellulose membranes and blocked for 5 hours at room temperature with milk (5% w/v) in Tris-buffered saline (TBS) with Tween-20 (0.1%; TBS-T). The blots were incubated with a primary antibody (1 : 200) directed against the Cav1.2 subunit overnight at 4°C with oscillation. The blots were incubated with horseradish peroxidase-conjugated secondary antibody (1 : 10,000; Jackson). The secondary antibodies were detected and visualized using the Super Signal West substrate (Fisher Scientific). Densitometry measurements were made using Tanon imaging software[61].

mRNA and miRNA expression assays. Total RNA from MC3T3-E1 was isolated using TRIzol reagent (Invitrogen). The concentration and purity of total RNA were determined by measuring the absorbance at 260 and 280 nm using a NanoDrop ND-1000 Spectrophotometer.

For mRNA, cDNA was synthesized using a Prime Script RT Kit (TaKaRa). The expression levels of target genes were determined quantitatively using an ABI 7500 real-time PCR system with SYBR Premix (TaKaRa). Amplification was performed for 40 cycles under the following conditions: 95°C for 45 s, followed by 40 cycles at 58°C for 45 s and 72°C for 60 s. The primers pairs were as follows: *Cacna1c* (GenBank Accession NM_009781): F-5′-TTG CCC TTC TTG TGC TCT TC-3′ and R-5′-TAT GCC CTC CTG GTT GTA GC-3′; GAPDH (NM_008084): F-5′-CAT GTT CCA GTA TGA CTC CAC TC-3′ and R-5′-GGC CTC ACC CCA TTT GAT GT-3′.

For miRNA, cDNA was synthesized using a miRNA First Strand Synthesis kit (Agilent Technologies). Then, an aliquot of the RT reaction was used as a template in a standard real-time RT-PCR amplification using SYBR Premix, the universal reverse primer 5′-TGG TGT CGT GGA GTCG-3′, and the miR-103 (mimat0000546)-specific forward primer 5′-ACA CTC CAG CTG GGA GCA GCA TTG TAC-3′. Amplification was performed for 40 cycles under the following conditions: 95°C for 2 min, followed by 40 cycles at 95°C for 10 s and 60°C for 40 s[31,50].

The quantification of gene expression was performed using the comparative threshold cycle ($\Delta\Delta C_T$) method. GAPDH was used as a control for Cav1.2 mRNA quantification, and small nuclear RNA U6 was used as a control for miRNA samples[35,62].

siRNA-mediated knockdown of Cav1.2. siRNA targeted against the murine *Cacna1c* sequence and a negative control siRNA with an irrelevant sequence were designed and synthesized by GenePharma. The siRNA sequences (*Cacna1c-mus-2942*) for *Cacna1c* were as follows: sense: 5′-GUG CCA CCG UAU UGU CAA UTT-3′; antisense: 5′-AUU GAC AAU ACG GUG GCA CTT-3′. The nonsense siRNA sequences were as follows: sense: 5′-UUC UCC GAA CGU GUC ACG UTT-3′; antisense: 5′-ACG UGA CAC GUU CGG AGA ATT-3′. Briefly, MC3T3-E1 cells were grown in α-MEM without antibiotics before siRNA treatment. The transfection medium was replaced after 5 h. Protein assays to assess knockdown were performed at 48 and 72 h after transfection. Functional assays were performed during maximum knockdown[61,62].

Synthesis and transfection of miRNA inhibitor. The miR-103 inhibitor was designed and synthesized by RiboBio Corporation. The sequence of miR-103 inhibitor is 3'-UCA UAG CCC UGU ACA AUG CUG CU-5'. Five nucleotides or deoxynucleotides at both ends of the antisense molecules were locked.

Osteoblasts were transfected with inhibitor or negative control using Lipofectamine 2000. The medium was replaced at 6 h after transfection. The cells were collected for protein assay or patch clamp at 48 h after transfection[35].

1. Duncan, R. L. & Turner, C. H. Mechanotransduction and the functional response of bone to mechanical strain. *Calcif Tissue Int* **57**, 344–358 (1995).
2. Nishizuka, Y. Intracellular signaling by hydrolysis of phospholipids and activation of protein kinase C. *Science* **258**, 607–614 (1992).
3. Riggs, B. L., Khosla, S. & Melton, L. R. A unitary model for involutional osteoporosis: estrogen deficiency causes both type I and type II osteoporosis in postmenopausal women and contributes to bone loss in aging men. *J Bone Miner Res* **13**, 763–773 (1998).
4. Yagodovsky, V. S., Triftanidi, L. A. & Gorokhova, G. P. Space flight effects on skeletal bones of rats (light and electron microscopic examination). *Aviat Space Environ Med* **47**, 734–738 (1976).
5. Morey, E. R. & Baylink, D. J. Inhibition of bone formation during space flight. *Science* **201**, 1138–1141 (1978).
6. Jee, W. S., Wronski, T. J., Morey, E. R. & Kimmel, D. B. Effects of spaceflight on trabecular bone in rats. *Am J Physiol* **244**, R310–R314 (1983).
7. Wronski, T. J. & Morey, E. R. Effect of spaceflight on periosteal bone formation in rats. *Am J Physiol* **244**, R305–R309 (1983).
8. Zerath, E. *et al.* Effects of spaceflight on bone mineralization in the rhesus monkey. *J Appl Physiol (1985)* **81**, 194–200 (1996).
9. Patterson-Buckendahl, P. *et al.* Fragility and composition of growing rat bone after one week in spaceflight. *Am J Physiol* **252**, R240–R246 (1987).
10. Doty, S. B., Morey-Holton, E. R., Durnova, G. N. & Kaplansky, A. S. Morphological studies of bone and tendon. *J Appl Physiol (1985)* **73**, 10S–13S (1992).
11. Zerath, E. *et al.* Spaceflight inhibits bone formation independent of corticosteroid status in growing rats. *J Bone Miner Res* **15**, 1310–1320 (2000).
12. Vico, L. *et al.* Effects of long-term microgravity exposure on cancellous and cortical weight-bearing bones of cosmonauts. *Lancet* **355**, 1607–1611 (2000).
13. Landis, W. J., Hodgens, K. J., Block, D., Toma, C. D. & Gerstenfeld, L. C. Spaceflight effects on cultured embryonic chick bone cells. *J Bone Miner Res* **15**, 1099–1112 (2000).
14. Pardo, S. J. *et al.* Simulated microgravity using the Random Positioning Machine inhibits differentiation and alters gene expression profiles of 2T3 preosteoblasts. *Am J Physiol Cell Physiol* **288**, C1211–21 (2005).
15. Bergh, J. J., Shao, Y., Puente, E., Duncan, R. L. & Farach-Carson, M. C. Osteoblast Ca^{2+} permeability and voltage-sensitive Ca^{2+} channel expression is temporally regulated by 1, 25-dihydroxyvitamin D_3. *Am J Physiol Cell Physiol* **290**, C822–C831 (2006).
16. Bergh, J. J., Shao, Y., Akanbi, K. & Farach-Carson, M. C. Rodent osteoblastic cells express voltage-sensitive calcium channels lacking a gamma subunit. *Calcif Tissue Int* **73**, 502–510 (2003).
17. Duncan, R. L., Akanbi, K. A. & Farach-Carson, M. C. Calcium signals and calcium channels in osteoblastic cells. *Semin Nephrol* **18**, 178–190 (1998).
18. Liu, R. *et al.* Ribozyme ablation demonstrates that the cardiac subtype of the voltage-sensitive calcium channel is the molecular transducer of 1, 25-dihydroxyvitamin D_3-stimulated calcium influx in osteoblastic cells. *J Biol Chem* **275**, 8711–8718 (2000).
19. Iqbal, J. & Zaidi, M. Molecular regulation of mechanotransduction. *Biochem Biophys Res Commun* **328**, 751–755 (2005).
20. Guggino, S. E., Lajeunesse, D., Wagner, J. A. & Snyder, S. H. Bone remodeling signaled by a dihydropyridine- and phenylalkylamine-sensitive calcium channel. *Proc Natl Acad Sci U S A* **86**, 2957–2960 (1989).
21. Ritchie, C. K., Maercklein, P. B. & Fitzpatrick, L. A. Direct effect of calcium channel antagonists on osteoclast function: alterations in bone resorption and intracellular calcium concentrations. *Endocrinology* **135**, 996–1003 (1994).
22. Vadiakas, G. P. & Banes, A. J. Verapamil decreases cyclic load-induced calcium incorporation in ROS 17/2.8 osteosarcoma cell cultures. *Matrix* **12**, 439–447 (1992).
23. Li, J., Duncan, R. L., Burr, D. B. & Turner, C. H. L-type calcium channels mediate mechanically induced bone formation in vivo. *J Bone Miner Res* **17**, 1795–1800 (2002).
24. Walker, L. M., Publicover, S. J., Preston, M. R., Said, A. M. & El, H. A. Calcium-channel activation and matrix protein upregulation in bone cells in response to mechanical strain. *J Cell Biochem* **79**, 648–661 (2000).
25. Li, J., Duncan, R. L., Burr, D. B., Gattone, V. H. & Turner, C. H. Parathyroid hormone enhances mechanically induced bone formation, possibly involving L-type voltage-sensitive calcium channels. *Endocrinology* **144**, 1226–1233 (2003).
26. Zanello, L. P. & Norman, A. 1α, $25(OH)_2$ vitamin D_3 actions on ion channels in osteoblasts. *Steroids* **71**, 291–297 (2006).
27. Ambros, V. The functions of animal microRNAs. *Nature* **431**, 350–355 (2004).
28. Bartel, D. P. MicroRNAs: genomics, biogenesis, mechanism, and function. *Cell* **116**, 281–297 (2004).
29. Bartel, D. P. MicroRNAs: target recognition and regulatory functions. *Cell* **136**, 215–233 (2009).
30. Fabian, M. R., Sonenberg, N. & Filipowicz, W. Regulation of mRNA translation and stability by microRNAs. *Annu Rev Biochem* **79**, 351–379 (2010).
31. Rau, F. *et al.* Misregulation of miR-1 processing is associated with heart defects in myotonic dystrophy. *Nat Struct Mol Biol* **18**, 840–845 (2011).
32. Zhang, Y. *et al.* Overexpression of microRNA-1 causes atrioventricular block in rodents. *Int J Biol Sci* **9**, 455–462 (2013).
33. Ripke, S. *et al.* Genome-wide association study identifies five new schizophrenia loci. *Nat Genet* **43**, 969–976 (2011).
34. Guella, I. *et al.* Analysis of miR-137 expression and rs1625579 in dorsolateral prefrontal cortex. *J Psychiatr Res* **47**, 1215–1221 (2013).

35. Lu, Y. *et al.* MicroRNA-328 contributes to adverse electrical remodeling in atrial fibrillation. *Circulation* **122**, 2378–2387 (2010).
36. Wang, J. *et al.* Differential expressions of miRNAs in patients with nonvalvular atrial fibrillation. *Zhonghua Yi Xue Za Zhi* **92**, 1816–1819 (2012).
37. Sadegh, M. K. *et al.* Deletion of Dicer in smooth muscle affects voiding pattern and reduces detrusor contractility and neuroeffector transmission. *PLoS One* **7**, e35882 (2012).
38. Favereaux, A. *et al.* Bidirectional integrative regulation of Cav1.2 calcium channel by microRNA miR-103: role in pain. *Embo J* **30**, 3830–3841 (2011).
39. Scott, A., Khan, K. M., Duronio, V. & Hart, D. A. Mechanotransduction in human bone: in vitro cellular physiology that underpins bone changes with exercise. *Sports Med* **38**, 139–160 (2008).
40. Wang, Y. C., Zhang, S., Du, T. Y., Wang, B. & Sun, X. Q. Clinorotation upregulates inducible nitric oxide synthase by inhibiting AP-1 activation in human umbilical vein endothelial cells. *J Cell Biochem* **107**, 357–363 (2009).
41. McAllister, T. N. & Frangos, J. A. Steady and transient fluid shear stress stimulate NO release in osteoblasts through distinct biochemical pathways. *J Bone Miner Res* **14**, 930–936 (1999).
42. Genetos, D. C., Geist, D. J., Liu, D., Donahue, H. J. & Duncan, R. L. Fluid shear-induced ATP secretion mediates prostaglandin release in MC3T3-E1 osteoblasts. *J Bone Miner Res* **20**, 41–49 (2005).
43. Chen, N. X., Geist, D. J., Genetos, D. C., Pavalko, F. M. & Duncan, R. L. Fluid shear-induced NFκB translocation in osteoblasts is mediated by intracellular calcium release. *Bone* **33**, 399–410 (2003).
44. Li, J., Duncan, R. L., Burr, D. B. & Turner, C. H. L-type calcium channels mediate mechanically induced bone formation in vivo. *J Bone Miner Res* **17**, 1795–1800 (2002).
45. Lieberherr, M. Effects of vitamin D_3 metabolites on cytosolic free calcium in confluent mouse osteoblasts. *J Biol Chem* **262**, 13168–13173 (1987).
46. Bidwell, J. P., Carter, W. B., Fryer, M. J. & Heath, H. R. Parathyroid hormone (PTH)-induced intracellular Ca^{2+} signalling in naive and PTH-desensitized osteoblast-like cells (ROS 17/2.8): pharmacological characterization and evidence for synchronous oscillation of intracellular Ca^{2+}. *Endocrinology* **129**, 2993–3000 (1991).
47. Duncan, R. L., Hruska, K. A. & Misler, S. Parathyroid hormone activation of stretch-activated cation channels in osteosarcoma cells (UMR-106.01). *Febs Lett* **307**, 219–223 (1992).
48. Yamaguchi, D. T., Green, J., Kleeman, C. R. & Muallem, S. Characterization of volume-sensitive, calcium-permeating pathways in the osteosarcoma cell line UMR-106-01. *J Biol Chem* **264**, 4383–4390 (1989).
49. Yang, L., Wang, Z., Wang, B., Justice, N. J. & Zheng, H. Amyloid precursor protein regulates Cav1.2 L-type calcium channel levels and function to influence GABAergic short-term plasticity. *J Neurosci* **29**, 15660–15668 (2009).
50. Ronkainen, J. J. *et al.* Ca^{2+}-calmodulin-dependent protein kinase II represses cardiac transcription of the L-type calcium channel α_{1C}-subunit gene (*Cacna1c*) by DREAM translocation. *J Physiol* **589**, 2669–2686 (2011).
51. Cui, J. *et al.* Correlation between oxidative stress and L-type calcium channel expression in the ventricular myocardia of selenium-deficient mice. *J Int Med Res* **40**, 1677–1687 (2012).
52. Wang, X. T. *et al.* Cardiac L-type calcium channel alpha 1-subunit is increased by cyclic adenosine monophosphate: messenger RNA and protein expression in intact bone. *J Bone Miner Res* **15**, 1275–1285 (2000).
53. Altier, C. *et al.* The Cavβ subunit prevents RFP2-mediated ubiquitination and proteasomal degradation of L-type channels. *Nat Neurosci* **14**, 173–180 (2011).
54. Rougier, J. S., Albesa, M., Abriel, H. &Viard, P. Neuronal precursor cell-expressed developmentally down-regulated 4-1 (NEDD4-1) controls the sorting of newly synthesized Cav1.2 calcium channels. *J Biol Chem* **286**, 8829–38 (2011).
55. Kacena, M. A., Todd, P., Gerstenfeld, L. C. & Landis, W. J. Experiments with osteoblasts cultured under varying orientations with respect to the gravity vector. *Cytotechnology* **39**, 147–154 (2002).
56. Barjaktarovic, Z. *et al.* Time-course of changes in amounts of specific proteins upon exposure to hyper-g, 2-D clinorotation, and 3-D random positioning of Arabidopsis cell cultures. *J Exp Bot* **58**, 4357–4363 (2007).
57. Ryder, K. D. & Duncan, R. L. Parathyroid hormone enhances fluid shear-induced $[Ca^{2+}]_i$ signaling in osteoblastic cells through activation of mechanosensitive and voltage-sensitive Ca^{2+} channels. *J Bone Miner Res* **16**, 240–248 (2001).
58. Takeuchi, K. & Guggino, S. E. 24R, 25-$(OH)_2$ vitamin D_3 inhibits 1α, 25-$(OH)_2$ vitamin D_3 and testosterone potentiation of calcium channels in osteosarcoma cells. *J Biol Chem* **271**, 33335–43 (1996).
59. Zanello, L. P. & Norman, A. W. Rapid modulation of osteoblast ion channel responses by 1α, 25$(OH)_2$-vitamin D_3 requires the presence of a functional vitamin D nuclear receptor. *Proc Natl Acad Sci U S A* **101**, 1589–1594 (2004).
60. Xie, M. J., Zhang, L. F., Ma, J. & Cheng, H. W. Functional alterations in cerebrovascular K^+ and Ca^{2+} channels are comparable between simulated microgravity rat and SHR. *Am J Physiol Heart Circ Physiol* **289**, H1265–H1276 (2005).
61. Thompson, W. R. *et al.* Association of the $\alpha_2\delta_1$ subunit with Cav3.2 enhances membrane expression and regulates mechanically induced ATP release in MLO-Y4 osteocytes. *J Bone Miner Res* **26**, 2125–2139 (2011).
62. Wang, H. *et al.* Chloride channel ClC-3 promotion of osteogenic differentiation through Runx2. *J Cell Biochem* **111**, 49–58 (2010).

Acknowledgments

We thank Prof. Tuck Wah Soong, Dr. Ping Liao, Dr. Jin Tao, Dr. Zipeng Cao and Dr. Jian Zhang for valuable suggestions regarding this work. This work was supported by grants from the National Science Foundation of China (31170889, 30870595, 81300928 and 81471815). The authors have no conflicts of interest to disclose.

Author contributions

Z.S., H.Z. and H.W. contributed to the biochemical assays. Z.S. and M.X. performed the electrophysiological experiments. S.Z., M.X. and Z.S. designed the experiments. Z.H., Z.L., X.C., D.L. and Z.S. analyzed the data. X.C. and Z.Z. prepared the figures. Z.S. and Z.Z. wrote the paper. All authors reviewed the manuscript.

Additional information

Competing financial interests: The authors declare no competing financial interests.

How to cite this article: Sun, Z. *et al.* Simulated microgravity inhibits L-type calcium channel currents partially by the up-regulation of miR-103 in MC3T3-E1 osteoblasts. *Sci. Rep.* **5**, 8077; DOI:10.1038/srep08077 (2015).